SF2A 2014
J. Ballet, F. Bournaud, F. Martins, R. Monier and C. Reylé (eds)

GALAXY CLUSTER DETECTION IN THE NEXT GENERATION VIRGO CLUSTER SURVEY (NGVS)

R. Licitra[1,2], S. Mei[1,2], A. Raichoor[1], T. Erben[3], H. Hildebrandt[3], O. Ilbert[4], M. Huertas–Company[1,2], L. Van Waerbeke[5], P. Côté[6], J.-C. Cuillandre[7], P.A. Duc[8], L. Ferrarese[6], S.D. J. Gwyn[6], A. Lancon[9], R. Munoz[9,10] and T. Puzia[10]

Abstract. We describe our cluster detection algorithm *Red–GOLD*, based on the search of red–sequence galaxy overdensities. In this work, the algorithm is optimized to search for clusters up to $z \sim 1$ using optical data. We applied this algorithm to semi–analytic simulations and we found that for haloes more massive than $M \geq 10^{14}\ M_{\odot}$ the completeness is 80% and the purity is $\sim 81\%$, up to redshift $z = 1$.

Keywords: galaxies, clusters, large survey

1 Introduction

Being galaxy clusters the most massive bound structures in the Universe, they represent a powerful tool to probe the large-scale structure predicted by the standard cosmological model, and to understand how environmental effects affect galaxy evolution. To conduct these studies and obtain reliable results, it is important to build complete and pure cluster catalogs.

2 Observations and data description

We applied our detection algorithm to optical data coming from the Next Generation Virgo Cluster Survey (NGVS), a *large program* on the *Canada France Hawaii Telescope* (CFHT), centred on the M87 galaxy and images the Virgo cluster from the inner regions up to its virial radius in 5 optical bands u^*, g, r, y, z, with a surface brightness depth of $\mu_g \sim 29/mag/arcsec^2$, never attained before in this region (Ferrarese et al. 2012).

The NGVS observations were carried out with MegaCam, the optical imager mounted on MegaPrime, the prime focus of the CFHT. For our analysis, we used the same reduction and photometric catalog as Raichoor et al. (2014). We refer to this last work for details. Briefly, the NGVS images were processed with the $ELIXIR^*$ pipeline at the Canadian Astronomical Data Centre (CADC†). The astrometric and photometric calibration, and the image co-addition and mask creation are described in Raichoor et al. (2014) and follow the reduction

[1] GEPI, Paris Observatory, 77 av. Denfert-Rochereau, 75014 Paris, France
[2] Université Paris Denis Diderot, 75205 Paris Cedex 13, France
[3] Argelander-Institut fur Astronomie, University of Bonn, Auf dem Hugel 71, D-53121 Bonn, Germany
[4] Aix Marseille Université, CNRS, Laboratoire d'Astrophysique de Marseille, UMR 7326, F-13388 Marseille, France
[5] Department of Physics and Astronomy, University of British Columbia, 6224 Agricultural Road, Vancouver, B.C., V6T 1Z1, Canada
[6] Herzberg Institute of Astrophysics, National Research Council of Canada, Victoria, BC, V9E 2E7, Canada
[7] CanadaFranceHawai Telescope Corporation, Kamuela, HI 96743, USA
[8] Laboratoire AIM Paris-Saclay, CEA/IRFU/SAp, CNRS/INSU, Université Paris Diderot, F-91191 Gif-sur- Yvette Cedex, France
[9] Observatoire astronomique de Strasbourg, Université de Strasbourg, CNRS, UMR 7550, 11 rue de l'Université, F-67000 Strasbourg, France
[10] Institute of Astrophysics, Pontificia Universidad Católica de Chile, Av. Vicuna Mackenna 4860, 7820436 Macul, Santiago,Chile
*http://www.cfht.hawaii.edu/Instruments/Elixir/
†http://www4.cadc-ccda.hia-iha.nrc-cnrc.gc.ca/cadc/

procedures from Erben et al. (2013). The photometric catalogs were obtained with the method described in Hildebrandt et al. (2012) with the global point–spread–function (PSF) homogenisation. Multi–wavelength catalogs were derived using SExtractor (Bertin & Arnouts 1996) in dual-image mode on each single pointing on the convolved images. The un–convolved y- band observations having the better average seeing ($0.52'' \pm 0.04''$), were chosen as detection images. Photometric errors were measured in the un–convolved images as described in Raichoor et al. (2014), from the noise estimation in 2,000 random apertures in each bandpass, in each pointing. In the un–convolved images, this corresponds to ~ 1.5 the photometric errors given by SExtractor. A zero point uncertainty, estimated comparing our photometry field–to–field and to the SDSS, was added in quadrature (see also Gwyn 2012).

The original NGVS observing strategy was to cover the entire field with the 5 bands (see Ferrarese et al. (2012)). However, due to the exceptionally bad weather, the observations in the r–band are available only on 34 out to 117 fields, which roughly correspond to 30 deg^2, and are shallower than originally planned.

3 Detection technique

Our algorithm, named Red-sequence Galaxy Overdensity cLuster Detector (*Red–GOLD*; Licitra et al., in preparation), is based on the detection of red-sequence galaxy overdensities: it relies on the observational evidence that red-sequence galaxies are tightly distributed in the colour-magnitude diagram, following an almost flat relation, at least up to redshift $z \sim 1.5$ (Blakeslee et al. 2006, Postman et al. 2005, Desai et al. 2007 Kodama et al. 1998 Muzzin et al. 2013 Mei et al. 2009). The use of high quality photometric redshifts described in Raichoor et al. (2014) allowed us to minimise projection effects.

The method consists in the detection of spatial overdensities of red early-type galaxies and the confirmation of a tight red-sequence in the colour-magnitude relation. To reduce the contamination due to projection effects when estimating the red–sequence galaxy overdensities, we selected passive galaxies using two pairs of filters simultaneously, roughly corresponding to the U-B and B-V rest-frame colours. We used Bruzual & Charlot (2003) (BC03) stellar population models to compute predicted colours through the theoretical Spectral Energy Distributions (SEDs): we assumed a passive evolution, a galaxy formation redshift $z_{form} = 3$ and a solar metallicity, $Z = 0.02$. In addition to our colour selection, we required that red galaxies are also defined as ETGs according to the spectral classification given by *LePhare* (Arnouts et al. (1999), Arnouts et al. (2002), Ilbert et al. (2006)), i.e. objects which show spectral characteristics typical of early-type galaxies.

We defined our cluster detections identifying structures with a high density contrast with respect to the mean value of the background. We centered our detections on a bright red ETG, considering the galaxy with the highest number of red companions, weighted on luminosity. This approach is compatible with previous analysis, showing that centroids do not well approximate the cluster centres, while the brightest cluster member lying near the X-ray centroid seems to trace very well the cluster centre (George et al. 2011, George et al. 2012). Finally, we confirmed our cluster candidates and refined our photometric redshift estimation, fitting the red–sequence and imposing upper limits for the red–sequence parameters, based on previous works (e.g., Mei et al. 2009). To remove multiple detections we iteratively filtered our catalogue, checking for detections characterised by at least half of members in common. Then, we simply retained only the detection with the highest signal–to–noise ratio, weighted on luminosity.

4 The NGVS cluster catalog

We applied this detection technique to the 104 deg^2 of NGVS to look for galaxy structures up to $z \sim 1$. We built two different cluster catalogues for fields with and without r–band observations, because we used a slightly different configuration, choosing different bands to isolate red–sequence galaxies.

4.1 Cluster catalogue with the r–band observations

We detected 287 structures in the ~ 30 deg^2 covered by the r–band, i.e. ~ 9 detections per square degree. The 62% of the cluster candidates have at least one spectroscopic member in less than $2'$ with $|z_{spec} - z_{cluster}| < 0.1$.

We compared our low-redshift detections with the red–Mapper catalog (Rykoff et al. 2014): red–Mapper has been applied to the SDSS data and we can use this catalog to empirically test the detections up to $z \sim 0.55$. We calculated how many red–Mapper detections are found with our algorithm. Of the 82 red–Mapper detections in the ~ 30 deg^2 covered by r–band observations, we recovered 80 clusters, i.e. the $\sim 98\%$ of the red–Mapper

cluster candidates. We checked for the two unmatched red–Mapper cluster candidates and from visual inspection we found that one is a poor system and the second lies on the edge of the NGVS field.

4.2 Cluster catalogue without the r–band observations

In the fields not covered by the r–band observations, we applied our algorithm considering different colour pairs as a function of redshifts, basically replacing the r–band with the y–band. With only four bands the photometric redshift estimates are more noisy (see Raichoor et al. 2014) but they remain accurate for our purposes. Therefore, we still used the photometric redshifts and the spectral classification to isolate red-sequence galaxies.

We found 864 cluster detections up to $z = 1$, i.e. ~ 10 clusters per square degree. 61% of the cluster candidates have at least one spectroscopic member in less than $2'$ with $|z_{spec} - z_{cluster}| < 0.1$.

When comparing our detections to the red–Mapper catalog, this comparison confirms that we are able to efficiently detect galaxy clusters also when using only four optical bands, recovering a similar fraction of the red–Mapper detections. Also in this case, when checking for the unmatched red–Mapper detections, we found that they are poor systems. With only four optical bands, though, we find it more uncertain to assign cluster membership, due to the higher photometric redshift uncertainties.

5 Completeness and purity of our algorithm from Millennium Simulation

We applied our detection algorithm to the Millennium Simulation (Springel et al. 2005). Among the different realisations of mock galaxy catalogues based on semi-analytical models, we used lightcones from Henriques et al. (2012), which consist in 24 independent catalogs, built on the models by Guo et al. (2011). Although, many improvements have been made with respect to previous simulations (e.g. the stellar mass function), the Guo models still show some discrepancies with the observations: in particular, galaxy colours are difficult to reproduce in an accurate way since they depends on different parameters, as metallicity, star-formation history and dust. Guo et al. (2011) showed that already at z=0, there is a discrepancy between the colours predicted in their models and the SDSS observations, overpredicting the fraction of red dwarf galaxies ($M < 10^{9.5}\ M_{\odot}$), with colours redder than observed. Instead, at $M > 10^{10.5} M_{\odot}$, the colours are bluer with respect to the observations. Moreover, assuming that ETGs are bulge-dominated, i.e. characterised by $B/T \geq 0.7$, we found that the early-type galaxy abundance in galaxy clusters is not well reproduced, systematically underestimating the fraction of early-type objects.

This deeply affects the comparison with results obtained with our algorithm, as it relies on the search of red-sequence galaxies and we have to take into account this effect. For that reason, we corrected mock catalogs in order to obtain a realistic galaxy distribution in simulated clusters and accurate colours.

In the upper panel of Figure 1, we show two examples of the colour-magnitude relation for two clusters at redshift $z = 0.23$ and $z = 0.93$: blue dots are cluster members, yellow triangles represent ETGs, i.e. members with $B/T \geq 0.7$, and red points are ETGs with colours in agreement with predicted ones, based on BC03 models. Both problems are clearly visible: the total number of ETGs is too small and only a small fraction of ETGs matches predicted colours.

Since we should consider colour cuts shifted with respect to the original BC03 predictions for both early and late type galaxies in all environments, we did not change the colours in the mock catalogues. Instead, we modified the colours predicted by BC03 stellar population models to match the Millennium galaxy colours to avoid to introduce biases in the galaxy large-scale properties. To do that, we identified early-type galaxies as objects with $B/T \geq 0.7$ and we defined a preliminary cluster catalogue in each lightcone as structures composed by at least 5 members, identified as objects characterised by the same FOF ID. We considered all bulge-dominated galaxies brighter than $0.2\ L^*$ in narrow redshift slices of 0.05 and we built the histogram of galaxy colours for each redshift bin. We fit this distribution with a Gaussian and we considered the mean $\bar{c}$ and the standard deviation σ_c of this distribution as a function of redshift. To apply appropriate color constraints, we imposed colour cuts in order to match the mean colour obtained from Henriques lightcones.

Moreover, for each cluster in the preliminary catalogue, we added a given fraction of early-type galaxies ($B/T \geq 0.7$): this fraction is a value randomly extracted from a Gaussian with a mean value $\bar{x} = 70$ and with $\sigma = 10$. For groups, we used the same prescriptions as for clusters, but we extracted values from a Gaussian with a mean value of 50 instead of 70 as for clusters. Finally, for field galaxies, we randomly modified a fraction of red galaxies to reach $\sim 30\%$ of ETGs at each redshift. We also added uncertainties to magnitudes, and redshifts, to reflect realistic photometry and photometric redshifts for the NGVS.

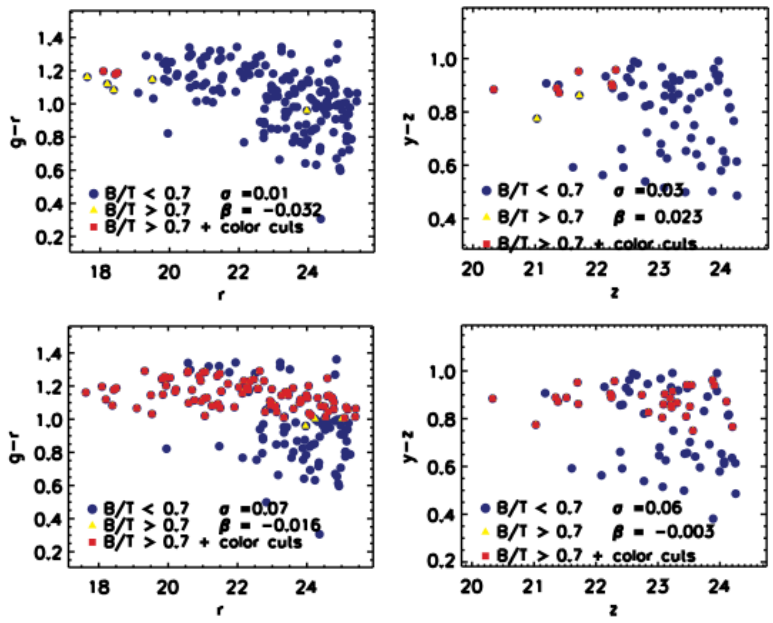

Fig. 1. Upper panel: colour-magnitude relation of two clusters in Henriques et al. (2012) lightcones at $z = 0.23$ and $z = 0.93$. Blue dots are cluster members, yellow triangles represent members with $B/T \geq 0.7$ and red points are ETGs characterised by colours in agreement with predicted ones from BC03 models. Lower panel: colour-magnitude relation for the same clusters, when predicted colours have been shifted and ETGs added.

When applying our detection method, we considered a colour cut around the mean colour $\bar{c} \pm 3\sigma_c$ corresponding at that redshift. In the lower panel of Figure 1, we show the corrected colour-magnitude-relation for the two clusters. Then, we run our detection code on mock catalogues to estimate completeness and purity, assuming the same requirements used with the NGVS sample: we found a completeness of $94\%, 80\%, 72\%, 35\%$ respectively at $M \geq 2 \times 10^{14}\ M_{\odot}, M \geq 10^{14}\ M_{\odot}, M \geq 5 \cdot 10^{13}\ M_{\odot}$ and $M \geq 1 \cdot 10^{13}\ M_{\odot}$ for $0.1 \leq z \leq 1.0$ while for $0.1 \leq z \leq 1.2$ we reach respectively $94\%, 75\%, 64\%, 33\%$ in completeness. In both cases, the overall purity is of $\sim 81\%$.

6 Conclusions

We presented the cluster detection algorithm *Red–GOLD* based on searching red–sequence galaxy overdensities, using colours and photometric redshifts and its application to the NGVS optical data. We found ~ 10 clusters per square degree up to $z \sim 1$. We tested our detection algorithm using semi-analytic simulations by Henriques et al. (2012): after correcting these lightcones to well reproduce the cluster red–sequence, we found a completeness of $94\%, 80\%$ up to $z = 1$, for clusters more massive than $M \geq 2 \times 10^{14}\ M_{\odot}, M \geq 10^{14}\ M_{\odot}$, respectively. Our estimated purity is $\sim 81\%$, at both mass limits.

References

Arnouts, S., Cristiani, S., Moscardini, L., et al. 1999, MNRAS, 310, 540
Arnouts, S., Moscardini, L., Vanzella, E., et al. 2002, MNRAS, 329, 355
Bertin, E. & Arnouts, S. 1996, A&AS, 117, 393
Blakeslee, J. P., Holden, B. P., Franx, M., et al. 2006, ApJ, 644, 30
Bruzual, G. & Charlot, S. 2003, MNRAS, 344, 1000
Desai, V., Dalcanton, J. J., Aragón-Salamanca, A., et al. 2007, ApJ, 660, 1151
Erben, T., Hildebrandt, H., Miller, L., et al. 2013, MNRAS, 433, 2545
Ferrarese, L., Côté, P., Cuillandre, J.-C., et al. 2012, ApJS, 200, 4
George, M. R., Leauthaud, A., Bundy, K., et al. 2012, ApJ, 757, 2

George, M. R., Leauthaud, A., Bundy, K., et al. 2011, ApJ, 742, 125
Guo, Q., White, S., Boylan-Kolchin, M., et al. 2011, MNRAS, 413, 101
Gwyn, S. D. J. 2012, AJ, 143, 38
Henriques, B. M. B., White, S. D. M., Lemson, G., et al. 2012, MNRAS, 421, 2904
Hildebrandt, H., Erben, T., Kuijken, K., et al. 2012, MNRAS, 421, 2355
Ilbert, O., Arnouts, S., McCracken, H. J., et al. 2006, A&A, 457, 841
Kodama, T., Arimoto, N., Barger, A. J., & Arag'on-Salamanca, A. 1998, A&A, 334, 99
Mei, S., Holden, B. P., Blakeslee, J. P., et al. 2009, ApJ, 690, 42
Muzzin, A., Wilson, G., Demarco, R., et al. 2013, ApJ, 767, 39
Postman, M., Franx, M., Cross, N. J. G., et al. 2005, ApJ, 623, 721
Raichoor, A., Mei, S., Erben, T., et al. 2014, ArXiv e-prints
Rykoff, E. S., Rozo, E., Busha, M. T., et al. 2014, ApJ, 785, 104
Springel, V., White, S. D. M., Jenkins, A., et al. 2005, Nature, 435, 629